

Novel Method for In-Flight Particle Temperature and Velocity Measurements in Plasma Spraying Using a Single CCD Camera

J. Vattulainen, E. Hämäläinen, R. Hernberg, P. Vuoristo, and T. Mäntylä

(Submitted 17 May 1999; in revised form 3 August 1999)

A novel, technically simple imaging system for individual, in-flight particle temperature and velocity measurements for plasma and other thermal spray processes is described. A custom double dichroic mirror is used to add spectral resolving capability to a single, black-and-white, fast-shutter digital charge coupled device (CCD) camera. The spectral double images produced by the individual in-flight particles are processed using specialized image processing algorithms. Particle temperature determination is based on two-color pyrometry, and particle velocities are measured from the length of the particle traces during known exposure times. In this paper, experimental results using the first prototype system are presented. Laboratory tests were performed using rotating pinholes to simulate in-flight particles, and plasma spraying experiments were performed with commercial, standard spraying equipment operated with Al_2O_3 and NiCrAlY powders. The prototype instrument can be readily used to determine velocity and temperature distributions of individual in-flight particles from the imaged region of interest of the plume. Dividing the imaged area into smaller sections, spatial distributions of particle temperature, velocity, and number of detected particles can be studied. The study aims to develop a technically simple, single imaging instrument, which can provide a visual overview of the spray plume in combination with quantitative evaluation of the most important spray particle parameters.

Keywords CCD camera diagnostics, imaging in-flight particle diagnostics, temperature, and velocity measurements

1. Introduction

In industrial applications of thermal spraying, the need to ensure constant coating quality and also the desire to reduce the overall process costs have generated a need for improved control of the process. The fundamental control parameters in plasma spraying are the flow rates of plasma and powder carrier gas, torch electric power, and powder port spatial adjustments together with the powder feed rate. The quality of the coating and the deposition efficiency are also influenced by any variations in the powder quality and in the condition of the electrodes and the nozzle of the spray gun. However, there exists no universal and unambiguous coupling between these control parameters and the final spray result that could be used to select the optimum process control parameters under given conditions. According to their nature, nonintrusive, optical measurement techniques provide the only practical way of obtaining *in-situ* information from the individual in-flight coating particles. Much research is, therefore, being devoted to the development of optical diagnostic methods to monitor the state of the spraying process.¹⁻⁵ Among the parameters of most interest are the par-

ticle temperature and velocity distributions, particle size distribution, and spatial distribution of particles in the plume.

Optical methods suitable to study the in-flight particles can be divided into point diagnostics versus imaging techniques and, further, into methods utilizing external illumination versus passive methods. The latter methods do not use additional light sources to detect the particles, but rely purely on the spontaneous light emitted by the hot particles themselves. The recent development of CCD cameras of reasonable cost and yet sufficient sensitivity and time resolution make these instruments very attractive for on-line monitoring purposes, especially in industrial applications where simple-to-use and rugged instruments are favorable. The possibility to obtain a visual overview of the spray plume in combination with quantitative evaluation of spray particle parameters underlines the attractiveness of imaging methods in comparison to measurement techniques, which provide essentially only point information from the plasma plume. The strength of imaging lies in its capability to submit an overall indication of anomalies in the spray pattern, which could be misinterpreted or not understood at all by point diagnostics. Such phenomena could include, for example, background radiation from bursts of plasma, clouds of fume originated from evaporating powder material, or collisions between in-flight particles. The integrated information from an extended region of the spray plume gives a more reliable indication of the trend of operational parameters than a measurement from one point of the plume only. For these reasons, and due to their relative technical simplicity and ease of use, the CCD imaging methods seem to have significant potential for process optimization and for continuous process monitoring during thermal spraying.

It has been demonstrated already that simple, passive, black-and-white CCD imaging together with modern digital image

J. Vattulainen, E. Hämäläinen, Oseir Ltd., Pinninkatu 53 B, FIN-33100, Tampere, Finland; R. Hernberg, Department of Physics, Plasma Technology Laboratory, Tampere University of Technology, FIN-33101 Tampere, Finland; and P. Vuoristo and T. Mäntylä, Institute of Material Science, Tampere University of Technology. Contact e-mail: esah@oseir.com.

processing can be used to determine the relative spatial particle concentration and particle velocities in plasma spraying and that these parameters correlate clearly with the coating quality.^[6,7,8] The expression “relative” refers here to the fact that information is received only from those particles, which are hot and large enough to be detected using the short, microsecond scale exposure times needed to freeze the motion of the particles. Exposure times in the nanosecond range together with order of magnitude higher optical magnification would be needed to reliably resolve particle sizes directly from the images. At the current state of CCD technology, this requires heavily light-intensified camera systems and is, therefore, because of both technical and economical reasons, more suitable to special laboratory use than for continuous use in an industrial environment.^[6] In addition to the particle velocity information, knowledge of the in-flight particle temperatures is essential for control of the spray process. Pyrometric methods have been commonly adopted already in the form of point measurements for the particle temperature determination.^[1–3,9]

The object of this paper is to discuss the possibility of adding spectral resolving capability to a single, black-and-white CCD camera system, and in this way to enable the use of imaging two-color pyrometry for individual particle temperature determination in plasma spraying. The study aims to develop a technically simple imaging instrument, which could provide a visual overview of the spray plume in combination with quantitative evaluation of the most important spray particle parameters.

2. Instruments

2.1 Measurement Principle

Figure 1 shows schematically the measurement setup developed in this work for spectrally resolved imaging of the individual in-flight spray particles based on their spontaneous light emission. The particles are imaged onto a CCD camera sensor with the aid of a custom designed dichroic double mirror. The front and back surfaces of the dichroic mirror are designed to reflect different spectral bands and the corresponding first and second reflections produce spectral two-color double images of single particles onto the CCD sensor. The orientation of the double mirror with respect to the CCD sensor is selected to produce an axial shift in the direction of the particle movement between the images from the first and second reflections. The mirror thickness and camera exposure time are selected to make the different wavelength band images of individual particles partially overlap each other in the middle. The purpose of this overlap is to help the particle identification and signal determination during the subsequent image processing.

Figure 2 describes schematically the determination of the double image signals needed for the quantitative particle parameter calculations. The upper curve in Fig. 2 shows an integrated line profile obtained from the double image using procedure, which is explained in detail in Section 3.2. In this curve, signals S_1 and S_2 , measured at different wavelength bands, are used to determine the particle temperature by applying the principle of two-color pyrometry.^[2,3,10–12,19] The middle part of the curve ($S_1 + S_2$) corresponds to the overlap of the images formed by the single particle. The lower curve showing peaks A–D is obtained from the upper integrated line profile curve using derivation. The

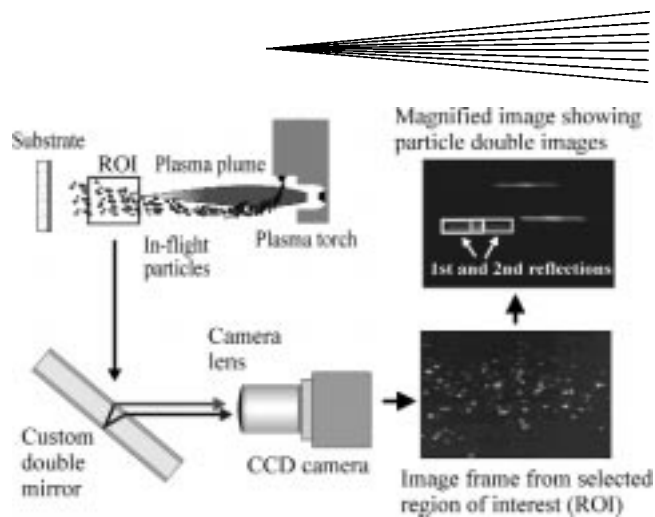


Fig. 1 CCD camera setup for spectrally resolved imaging of the in-flight spray particles

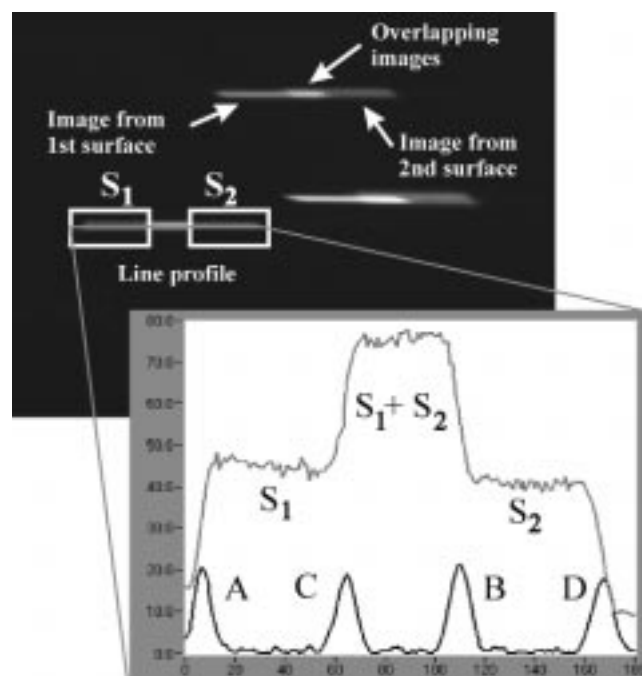


Fig. 2 Signals determined from a double image of an individual spray particle for subsequent temperature and velocity determination. The upper curve shows an integrated line profile obtained from the double image using procedure, which is explained in detail in Section 3.2. The lower curve showing peaks A–D is obtained from the upper integrated line profile curve using derivation

distances between the derivative signal peaks, A to B, or C to D, give the length of the particle trace during the known exposure time and are used for particle velocity determination. The trace of the particle in the image frame can also be used to determine the direction of the particle movement with respect to the fixed position of the camera. The absolute values of the particle and background signal levels together with the properties of the derivative signal peaks are used for particle image classification prior to temperature and velocity determination. This classification is needed to analyze only particles that have high enough

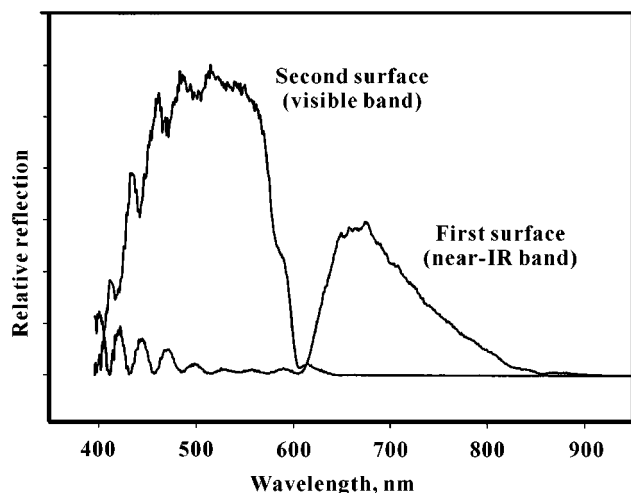


Fig. 3 Reflectance spectra of the first and second surfaces of the dichroic double mirror

signal-to-noise ratio, are sufficiently well focused, are isolated from any other nearby particles, and are not blocked due to other particles in the line-of-sight.

2.2 Dichroic Double Mirror and Imaging Optics

The reflectance spectra of the first and second surfaces of the dichroic double mirror are shown in Fig. 3. The mirror was custom manufactured (Oplatek Ltd, Leppävirta, Finland) by depositing multilayer dielectric coatings onto a 0.9 mm thick glass plate substrate.

The thickness of the mirror was selected to generate suitable image separation on the CCD sensor together with optical magnification of the camera lens, which was found appropriate for the visualization of the in-flight particles during the earlier studies.^[6-8] The selected 0.9 mm thickness was also found to provide sufficient mechanical rigidity for the mirror. The spectral bandwidths were designed to be wide to compensate for the limited sensitivity of the CCD sensor. The relative transmission of the wavelength bands was designed to produce close to a 1:1 signal ratio at the typical temperatures found in thermal spraying, and especially in plasma spraying processes, taking into account also the effect of the camera lens transmission and the CCD spectral sensitivity.

The camera lens used in the prototype system is a standard 35–105 mm zoom lens (Nikon Nikkor AF, Tokyo, Japan) equipped with additional +2 or +4 diopter close-up lenses. The close-up lenses are used to achieve wider lens-to-object distance maintaining at the same time the required image magnification. In typical plasma spraying experiments, the width of the imaged region of interest (ROI in Fig. 1) in the plasma plume has been from 20 to 30 mm, and the corresponding height 16 to 24 mm. When using a 2/3 in. format CCD chip having an effective optically active area of 8.8×7.0 mm, this corresponds to optical magnification between 0.44 and 0.29.

The non-negligible thickness of the dichroic mirror gives rise to an optical path difference between the images from the first and second surface reflections. However, the camera lens also has an axial chromatic aberration when operated with the wave-

Table 1 Technical specifications of the digital CCD camera used in the prototype system

Sensor format	2/3-inch CCD black-and-white
Number of pixels	1280 × 1024 (horizontal × vertical)
Unit pixel size	$6.7 \times 6.7 \mu\text{m}$
Spectral range	290–1000 nm
Exposure time	100 ns–10 ms
Maximum frame rate	7 frames/s
Dynamic read-out range	12 bits, 4096 gray levels
Full well charge capacity	25,000 electrons
A/D conversion factor	5 electrons/count
Read-out noise	7–8 electrons/readout
Average dark charge	0.1 electrons/pixel in second
Signal nonlinearity (photons to charge)	<0.3%
Spatial nonuniformity in darkness	typical 1 count
Spatial nonuniformity in brightness	typical 0.6%
CCD temperature stabilization	–12°C (Peltier cooling)

length bands shown in Fig. 3. In practice, it was found that the path difference of the mirror could be used to compensate for the axial chromatic aberration of the lens. The performance of the mirror and the lens together is better than that of the lens alone, and thus sufficient for this application.

2.3 CCD Camera Characteristics

During earlier studies,^[6-8] different types of CCD cameras have been tested for the in-flight particle imaging in plasma and thermal spraying. A nonintensified, black-and-white CCD camera was chosen here, because this study aims to develop a technically simple and rugged imaging instrument suitable for industrial environments. The camera mainly used during earlier work was an analog video camera (Flashcam, PCO Kelheim, Germany) equipped with a fast electronic shutter (1 μs to 10 ms) and with 756×580 pixel resolution. The need for accurate signal determination required in this study for the pyrometric temperature measurement cannot, however, be met by using analog video signal transfer. When using an analog video signal, the final effective read-out accuracy of the A/D conversion at the frame-grabber board in the PC computer is normally below 256 gray levels (8-bit), and also the dark signal level and overall signal-to-noise ratio tend to be rather high. The signal fidelity of the analog transfer signal can be further affected by electromagnetic interference produced by the high current plasma arc.

The camera selected for this study is a 4096 gray level (12-bit) digital read-out camera (Sensicam SVGA, PCO Kelheim, Germany), where the signal from the camera is transferred to the PC computer in digital format via a fiber optic link. The CCD sensor of the camera has 1280×1024 pixels and is Peltier cooled to reduce dark signal level, and also to stabilize the overall sensitivity of the CCD. Technical specifications of the camera and the detector are given in Table 1.

The CCD sensor of the camera is an interline progressive scan CCD (Sony ICX085AL, Japan) together with lens-on-chip technology.^[13] Some prime features of this type of a CCD detector are provided as background for the discussion concerning the accuracy limitations in single particle imaging (Section 3.1).

The major advantage of an interline progressive scan CCD detector, and the fundamental requirement in this application, is

Table 2 Specifications of the computer and software used in the prototype system

CPUs	2 × 350 MHz Pentium II
Memory	256 MB RAM/12.8 GB hard disk
Platform	Windows NT
Image processing software	Labview + IMAQ Vision Toolkit
Frame processing rate	typical 2 full frames/s

that it provides simultaneous electronically controlled exposure time over the full frame without any external shutter mechanism. This feature is essential to be able to construct reliable, full frame, fast electronic shutter ($< \mu\text{s}$) CCD cameras at reasonable cost. As a drawback, due to the intermediate storage and control structure areas between the adjacent pixels, the complete sensor area is not light sensitive. Typically, the light sensitive surface covers approximately 30% of the area of a single pixel unit. This effect can be compensated for by using a lens-on-chip technique, where a microlens is placed over every sensor cell of the chip to capture the light, which would otherwise fall onto the inactive areas of the pixel unit. Using this technique, the active area of the single sensor is roughly doubled from 30% to 60 to 70%.

To sum up the most important nonideal features of a CCD detector concerning this type of application, the sources of error can be divided into two main categories. First, an interline progressive scan CCD has less than 100% active pixel area. Second, a certain minimum amount of photons are needed in each pixel to exceed the detection threshold due to the above discussed inherent sources of noise.^[14,15] These characteristics of the sensor have to be taken into account, when considering the optimum method of imaging small and fast moving single particles in thermal spraying applications.

2.4 Application Software and Computer

A single, full resolution CCD image recorded with the prototype setup contains a total of over 1.3 million pixels and occupies 2.5 megabytes of memory space. When the information of the individual particles contained in such images is processed on-line to make the real-time process monitoring possible, this requires use of efficient computer hardware and software solutions. Taking into account both practical and economical points of view, the prototype data processing was based on standard PC computer technology and commercial image processing software. Table 2 shows the main specifications of the computer and software used in the prototype.

Labview (National Instruments Austin, USA) is a widely used graphical programming language for instrumentation applications. IMAQ Vision Toolkit (National Instruments) contains additional high-level machine vision and image processing functions. The main benefit of this approach was an effective application program development, which included a capability to create easy-to-use user interfaces. The in-house written application software employs parallel processing using two separate CPUs and enables remote control of all camera settings.

Using the equipment specified here, the prototype system captures and processes two full image frames per second performing all necessary image processing together with on-line presentation of the particle parameters. Depending on the situa-

tion, the number of particles accepted for final processing in a single image taken from the ROI varies from a minimum of a few particles to several hundred particles. In a typical plasma spraying situation, single particle information is obtained at 50 to 200 Hz.

3. Data Processing

3.1 Single Particle Imaging onto CCD Pixels

The selection of the magnification of the lens optics is a compromise between imaging a rather large and representative part of the plasma plume and being, at the same time, able to resolve reliably the images of single particles using the available pixel resolution of the CCD sensor. Imaging a single particle onto a minimum number of pixels is advantageous in achieving maximum detectivity and high signal-to-noise ratio, because then a minimum portion of the available photons is used to reach the detection threshold in those pixels. Before reaching the threshold, the photons are lost without creating measurable increase in the pixel signal values. Dividing the light onto a larger amount of pixels increases the number of ineffectively used photons created in this way. On the other hand, if only a small number of pixels are used, then the lower-than-100% active area of the pixels can affect significantly the signal determination. The ratio of the spectral signals measured from the double image of a particle for the temperature determination can change depending on how these images are located with respect to the active areas of a few individual pixels. If the number of illuminated pixels is higher, then the number of pixels on the edge of the image compared to the number of pixels within the image becomes small. This causes the two spectral signal values to be reduced still by a constant factor corresponding to the active pixel area divided by the area of the entire pixel unit, but it leaves the ratio of the spectral signals effectively unchanged.

Typical optical magnifications used in this study were between 0.29 and 0.44. When the magnification of the lens optics is, for example, 0.3, a stationary $30 \mu\text{m}$ particle will, assuming ideal optical imaging properties, produce a $10 \mu\text{m}$ diameter image on the CCD sensor surface. With a unit pixel size of $6.7 \times 6.7 \mu\text{m}$, the light would then fall onto only a few pixels. In practice, the movement of the in-flight particles causes the light to distribute over a larger number of pixels when the images of particles sweep over the sensor surface during the camera exposure time. This effect also determines an effective exposure time for the individual pixels, which is shorter than the gate time set to the camera. For example, if a particle is moving 250 m/s and the camera gate is set to $5 \mu\text{s}$ exposure, then using an optical magnification of 0.3, the particle image moves a distance of $375 \mu\text{m}$ across the CCD sensor during the exposure. This distance corresponds to approximately 56 pixels in the prototype system used here.

In addition to the movement of the particles, the sharpness of the focus of the particle images also influences the amount of illuminated pixels per particle. In the actual measurements using the prototype system, the individual particle images are thus formed by a minimum of several dozen up to a few hundred pixels. This decreases the significance of the effect of the nonactive areas of the pixel units, but increases the portion of light needed

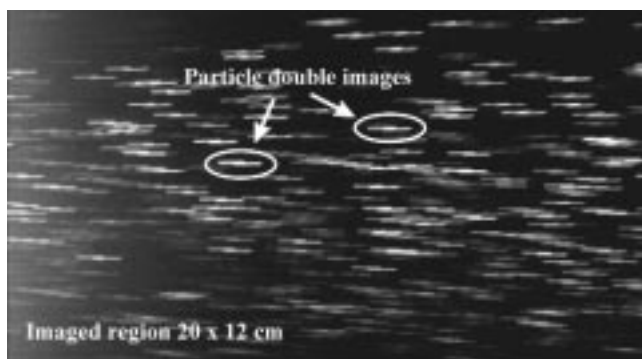


Fig. 4 Typical raw image frame from plasma spraying of Al_2O_3 showing double images of single particles

to achieve the detection threshold in the numerous pixels. If the spectral images produced by a single particle have the same size, the latter effect would not, in theory, change the ratio of the spectral signals. However, due to the achromatic effects of the imaging optics, this cannot be realized in practice. These effects will be discussed further in Section 4.1.

3.2 Particle Detection Algorithms

The orientation of the double mirror with respect to the CCD sensor is selected to produce an axial shift in the direction of the particle movement between the images from the first and second reflections. It is also possible to produce a vertical lateral shift between the images, but in practice it was found that the axial shift with some overlap in the single particle images is advantageous during the subsequent image identification and signal determination.

The original frame taken from the plasma plume represents the raw data that have to be filtered and processed to extract the quantitative information. A typical raw image frame from plasma spraying of Al_2O_3 powder is shown in Fig. 4.

The double images of the individual particles are clearly visible in the frame, but they differ in intensity, level of focusing, length, and orientation. Particle image pairs are randomly distributed over the frame and may also be partially overlapping. In addition, there is a background due to out-of-focus particles and, possibly, emitting gases. Thus, the image processing methods should first classify the particle images so that clearly overlapping and badly focused images are rejected. In the next phase, the potentially valid particle images are further processed to recognize different parts of the image to determine the signals needed for analysis of temperature, velocity, and orientation.

Figure 5 shows schematically the first treatment of the image frame used to determine the coordinates of the potentially valid particles in the original frame. The single frame containing 1280×1024 pixels is resampled to produce a quarter size (640×512 pixel) reduced frame. This is necessary because the subsequent convolution filtering and thresholding operations are performed on every pixel of the frame and become very time consuming if applied to the original large frame. Convolution filtering is a form of spatial filtering, where the new value for each pixel is determined based on the intensity of the pixel and its neighborhood. Here, convolution filtering is used for enhancing

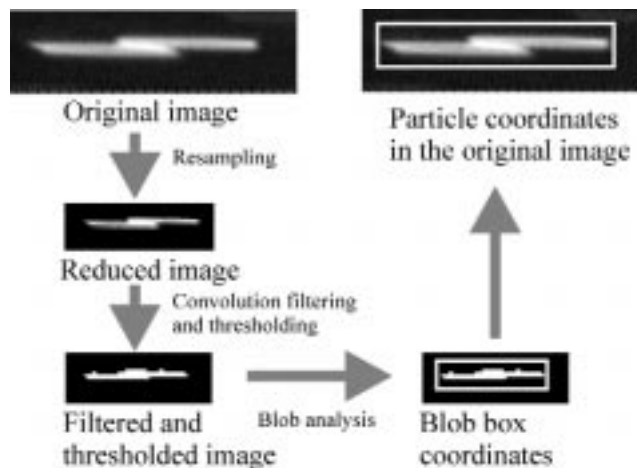


Fig. 5 First phase processing of the single particle images in the frame

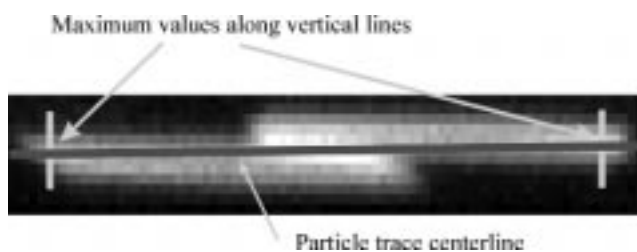


Fig. 6 Locating the centerline of the double particle trace image

the edges of the particles and for smoothing and noise reduction. Thresholding the frame after the convolution operation produces a binary image frame, where the particles have pixel values of unity and the background intensity is set to zero. This binary image frame is then used for blob analysis, where well-defined, distinct constant value areas, *i.e.*, blobs, are classified according to their area and length. Blobs with too small an area are rejected, because they represent particle images that have been split into two or more parts during the filtering process. These particles are poorly visualized in the original images and are not appropriate for temperature and velocity determination. Very long blobs are abandoned too, because they are likely to represent two overlapping images from different particles. Coordinates of the accepted particles are derived from the blob box coordinates of the reduced frame by multiplying them with the same factor by which the original image was reduced.

After determining the coordinates of the potentially valid particles in the original frame, each particle image is further examined separately. The double image of each particle is in the next phase analyzed using signal line profile techniques described in the following. First, the orientation of the particle centerline is determined by taking vertical line profiles from the ends of the particle image and by finding the y -coordinates corresponding to the maximum values in those profiles. This is schematically shown in Fig. 6.

When the centerline is found, a wider integration border is created along the centerline and an integrated signal line profile is calculated along the centerline. This is shown schematically

in Fig. 7 for a sharply focused particle and also for comparison for an out-of-focus particle. The profile is integrated in every x -position of the centerline over the width of the border in the y -direction area in order to measure the total light emitted by the particle. The purpose of the integration is to make the signal determination less sensitive to the state of particle focusing.

In Fig. 7, the signal line profile is shown together with the background signal level. The algorithm determines the background signal by averaging the signal values in the ends of the line profile outside the particle image. To accept the particle for further processing, the background signal measured at both ends must be equal within a given tolerance, typically within a few percent. Typically, Fig. 7 shows also the derivative signal calculated from the integrated line profile. The beginning and end of the different spectral sections of the double image can be found by identifying the locations of the corresponding peaks in the derivative signal. To be accepted as a valid particle, results of peak detection must fulfill the following conditions. First, there must be exactly four peaks exceeding a given threshold level in the derivative signal. Second, the distance between peaks A and B, and the distance between C and D (Fig. 7), must be equal within an acceptable tolerance. Finally, the peaks A and B, or similarly C and D, must not be too close to each other. In practice, these criteria give an effective and reliable way to discriminate between good and unacceptable particle images. The conditions for the number of peaks and minimum distance between the peaks ensure that there are no overlapping particles in the image. The condition for the peak height controls the focusing level of the particle. For out-of-focus particles, the peaks in the difference signal become shallower than the sharp peaks produced by well-focused particles.

For the finally accepted images, particle velocity can be straightforwardly calculated from the distance between the peaks A and B, or C and D, respectively, knowing the exposure time of the camera and the magnification of the optics. The two-color pyrometric signal needed for particle temperature determination is the ratio of intensities S_1 and S_2 . Signals S_1 and S_2 are calculated by summing the integrated intensity values from comparable areas between the peaks A and C, and correspondingly B and D, in the integrated line profile. The background signal is subtracted from these signals before temperature determination.

4. Experimental Results

4.1 Laboratory Tests with Pinhole Simulator

Preliminary development of the particle detection algorithms and testing of the particle temperature measurement accuracy were performed in the laboratory using a simulator setup shown schematically in Fig. 8. The image of the filament of a calibrated tungsten ribbon lamp (Osram W14G, München, Germany) was imaged onto a rotating disk. The double mirror imaging system was focused onto the plane of this disk from the opposite side. The disk was furnished with 50 to 100 μm pinholes to simulate hot spray particles. The size and the virtual temperature of the pinholes are effectively of the same order as those of the spray particles, but the velocity of the simulated particles is significantly lower, being only on the order of 10 m/s due to the limited rotational velocity of the disk. Low f -number, parabolic

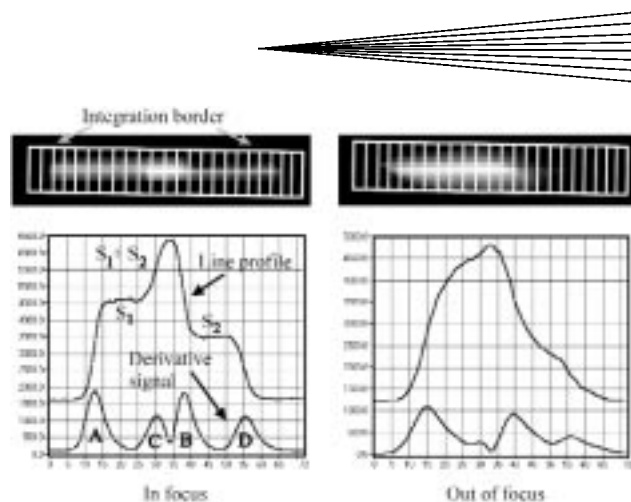


Fig. 7 Integrated single line profile and derivative signal from the double particle image. On the left side signals for a sharply focused particle, and on the right side for an out-of-focus particle

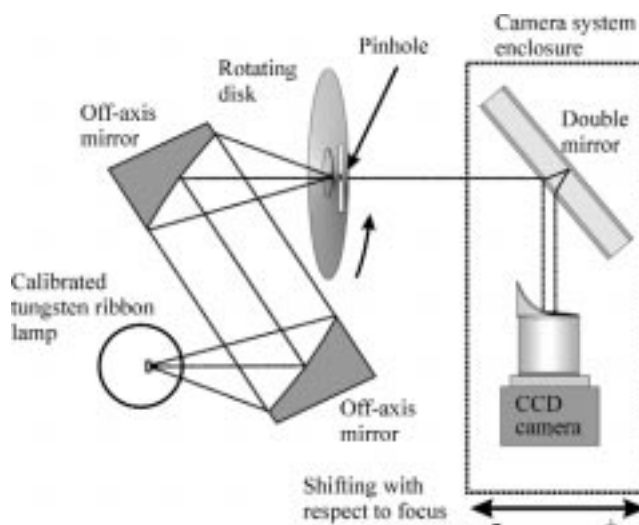


Fig. 8 Rotating pinhole simulator for particle detection algorithm development and for testing the accuracy of the particle temperature determination

off-axis (angle 60° , aperture 50 mm, and focal length 68 mm) mirrors were used to focus the filament onto the disk without chromatic aberration.

The temperature calibration of the double mirror imaging system was performed by replacing the moving pinholes with a stationary rectangular slit (1×2 mm) to achieve optimal signal-to-noise ratio. The ratio of the two spectral signals was determined as an average over the area of the corresponding images of the slit. This signal ratio was further recorded as a function of the lamp current and, thus, as a function of known filament temperature. A polynomial was fit into the calibration data, and the resulting calibration curve giving temperature as a function of the signal ratio was stored in the computer memory.

When testing the accuracy of the particle temperature measurement using the moving pinholes, the objective of the simulation was twofold. First, it was used to determine the effect of small object imaging onto the CCD pixels discussed earlier in

Table 3 Results of the rotating pinhole measurements performed with the imaging system focused onto the disk and with and without using the random delay in the camera trigger. Exposure time was 110 μ s and values are from 200 simulated particles per measurement

Calibration lamp settings		With random delay trigger		With constant trigger	
Current (A)	T_{lamp} (K)	T_{pinhole} (K) average	T_{pinhole} (K) standard deviation	T_{pinhole} (K) average	T_{pinhole} (K) standard deviation
12.00	2333	2305	44	2299	42
13.00	2431	2415	39	2401	33
14.00	2518	2511	39	2508	33
15.00	2631	2622	42	2604	29
16.00	2746	2724	41	2738	37

Section 3.1. To test this effect, the camera was triggered using a random delay, which caused the pinhole images to be located randomly within a different group of individual pixels in different frames. Second, the imaging system was shifted parallel along the optical axis to move the focal plane with respect to the location of the rotating disk and the pinholes. This was done to determine the degradation of the temperature measurement accuracy when measuring out-of-focus particles. To simulate a real situation better, this experiment was performed using the random delay in the camera trigger.

Table 3 shows the results of the rotating pinhole simulation measurements performed with the imaging system focused onto the rotating disk with and without using the random delay in the camera trigger. For each temperature T_{lamp} of the calibration lamp ribbon, the measured average temperature of 200 simulated particles, T_{pinhole} , is given together with the corresponding standard deviation. The exposure time used in these measurements was 110 μ s.

Table 3 shows that the recorded average temperatures of the simulated particles correspond within a few percent accuracy to the temperature of the calibration lamp. The systematic trend to measure slightly underestimated average temperatures was found to be due to the drift of the calibration lamp and current source properties between the calibration of the system and the actual pinhole measurements. The standard deviations recorded using a random delay trigger are slightly higher than those recorded using a constant trigger. In this temperature range, the uncertainties represented by the standard deviation values correspond typically to a few percent of the recorded temperatures. During the calibration measurements, using the larger area slit, the standard deviations corresponded on the order of $\pm 5^\circ$ in this temperature range.

Figure 9 shows results of the rotating pinhole simulation measurements performed by varying the focal plane of the imaging system with respect to the location of the pinholes. For a given constant temperature of the calibration lamp (2518 K), 200 simulated particles were measured for each point using 110 μ s exposure time and the random delay trigger.

From Fig. 9, it can be seen that there is a trend in the measurement error of the average temperatures as a function of deviation from focus. The cause of this trend is explained in the following. In the best focus condition (0 mm), the optics are adjusted in such a way that the two images at different wavelength

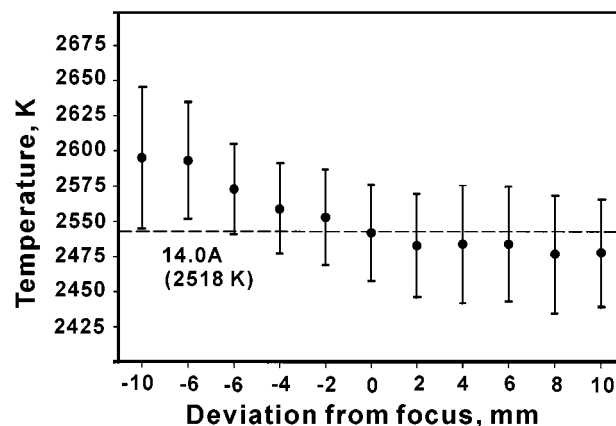


Fig. 9 Results of the rotating pinhole measurements performed varying the focal plane of the imaging system with respect to the location of the rotating disk and pinholes. Average values from 200 simulated particles per measurement are shown as black dots and corresponding standard deviations are given as error bars. Exposure time was 110 μ s. Negative deviation values correspond moving closer to the disk and positive values vice versa

bands originated from the single particle have similar sizes on the CCD surface. In practice, this also means that neither of these images have the smallest possible image size; *i.e.*, the focus is not optimum at this location. Therefore, when moving away from this zero point, the ratio of the area of the visible and near-infrared particle images on the CCD changes. The solid angle of the light collection changes also, but this change is similar for both spectral images. At negative displacements, the area of the infrared image is larger than that of the visible image, and at positive displacements, *vice versa*. In the case of an ideal detector, the change of the image size would be compensated fully by the integration of the signal from all illuminated pixels, but in the case of a real CCD detector, this cannot be entirely realized. When the light is divided into larger amounts of pixels on the CCD, a larger amount of photons is also required to exceed the minimum detectable signal level in each pixel. Thus, a relatively larger part of the photons is wasted without creating a measurable increase in the signal integrated from the illuminated pixels. At negative displacements, this reduction of signal takes place more severely in the infrared image, thus leading into a slight increase in the two-color temperature. At positive displacements, the same effect causes the visible signal to be underestimated, which causes the temperature value to fall short of the true temperature.

In a real measurement situation, the relatively poor particle image quality produced by larger deviations than approximately ± 5 mm leads to rejection of those particles using the methods described in Section 3.2. Therefore, in practice, maximum errors caused by the out-of-focus effects to the average temperatures in this temperature range are of the order of ± 25 K. Because the final results are averaged over the line-of-sight, in practice, the resulting error in the average temperatures is further compensated.

To test the capability of the imaging system to resolve small changes in the particle temperature, rotating pinhole measurements were performed by changing the lamp current in 0.1 A

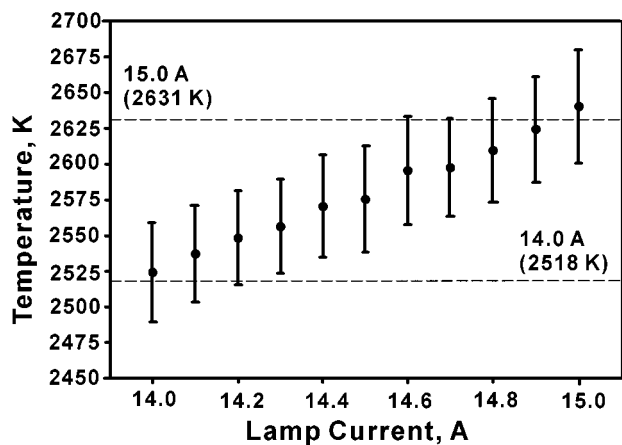


Fig. 10 Results of the rotating pinhole measurements performed with the imaging system focused onto the disk and changing the calibration lamp current in 0.1 A steps between 14.00 and 15.00 A. Exposure time was 110 μ s and measurements were performed using the random delay in the camera trigger. Average values from 200 simulated particles per measurement are shown as black dots and corresponding standard deviations are given as error bars

Table 4 Plasma spray parameters used in the experiments. Slightly different parameters were used during the spectral measurements and are given in the text

Powder type	Al ₂ O ₃ (A6060)	NiCrAlY (A962)
	fused and crushed	spherical
Powder size (μ m)	5–45	53–106
Nozzle diameter (mm)	6	6
Injector diameter (mm)	1.5	1.8
Current (A)	600	600
Power (kW)	42.6	40.8
Argon flow (slpm)	41	65
Hydrogen flow (slpm)	14	14
Argon carrier flow (slpm)	3.4	2.7
Powder feed rate (g/min)	34	60
Measurement/spray distance (mm)	120	140

steps between 14.00 A (2518 K) and 15.00 A (2631 K). Results of this test are shown in Fig. 10 using averaging over 200 simulated particles per measurement point, random delay in the camera trigger, and 110 μ s exposure time. A 0.1 A change in the lamp current corresponds to a change of 10°, approximately, in the filament temperature. From Fig. 10, it can be seen that these changes in the average temperature can be reliably detected in this temperature range.

4.2 Plasma Spraying Experiments

Plasma spraying experiments were performed using F4 plasma guns (Sulzer Metco, Wohlen, Switzerland) operated under the spray parameters presented in Table 4.

The application of pyrometric temperature measurement to plasma-sprayed particles is based on the assumption that effectively only radiation, which is thermally emitted by the particles under observation, is collected with the measurement device. However, in reality, the collected light is composed of different

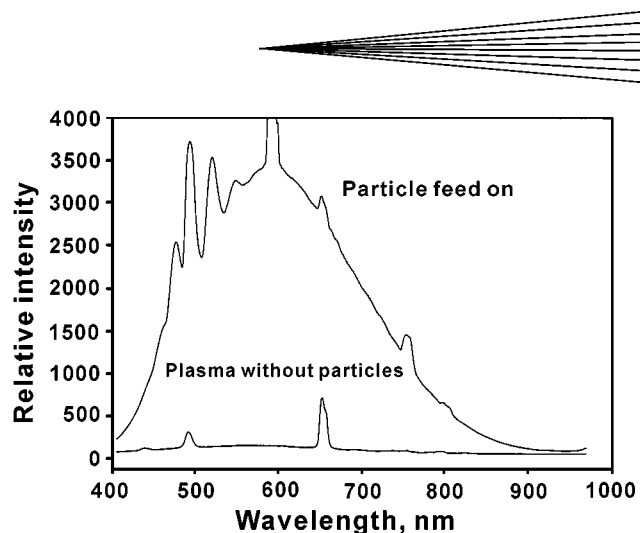


Fig. 11 Spectra recorded at distance of 110 mm from the nozzle of a F4 plasma torch without and with particle feed (Al₂O₃).

components: the thermal radiation from the particles, the light emitted by the plasma in the measurement volume, and the light scattered by the particles irradiated by the plasma arc and the surrounding emitting gases and neighboring particles. The ratio between the intensities of these different sources of light influences the accuracy of the temperature measurement.^[16,17]

Prior to the in-flight particle temperature measurements, this effect was studied by performing spectrally resolved measurements using a transmission diffraction grating spectrograph (Im-Spector V10, Specim Ltd., Oulu, Finland) attached between the digital camera and the camera lens.^[18] The lens settings (magnification 0.38) were kept similar to the ones for typical plasma spray measurements. The spectrograph had a 50 μ m wide entrance slit located on the focus plane of the camera lens. During the measurements, the entrance slit was aligned laterally across the plasma plume at the spraying distance, thus determining a 130 μ m wide measurement volume laterally across the plume. The spectral image of this measurement volume was formed through the spectrograph onto the CCD.

During the spectral measurements, the spraying parameters were slightly different than presented in Table 4. The powder was Al₂O₃ (Amperit 740.1) with a particle size range of 22.5 to 44 μ m, and the powder port diameter was 1.8 mm. The arc current was also slightly higher (610 A and 44.6 kW) than given in Table 4. The spectra were recorded at the distance of 110 mm from the nozzle exit.

Figure 11 shows the emission spectra recorded from the plasma with and without particle feed. The effective spectral resolution of the measurement was 3.5 nm. The lower curve recorded without particles shows a relatively weak continuum together with two noticeable spectral peaks. The upper curve recorded with the particle feed on shows a strong blackbody continuum originating from the hot particles together with some clearly distinguishable spectral line features. When integrating the signal over the measurement bandwidths of the imaging system (Fig. 3), however, the portion of the signal coming from the spectral lines is small compared to the continuum signal. The strongest spectral peak can be identified to be due to Na (589.0 and 589.6 nm), which is contained in the powder in small quantities as an impurity. Even very small quantities of Na can cause

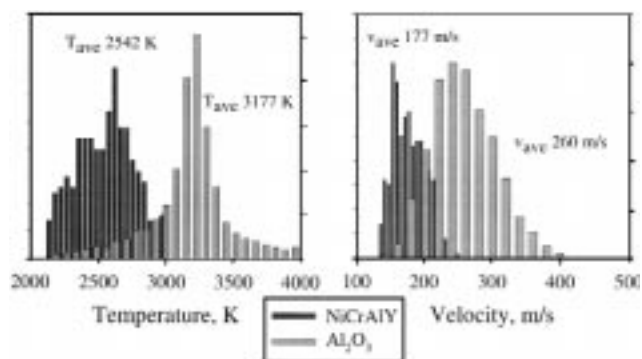


Fig. 12 Temperature and velocity of plasma sprayed Al_2O_3 and NiCrAlY particles recorded using the double mirror imaging system. Spray parameters are given in Table 4

strong interfering spectral lines, and therefore, the change of the reflectance of the dichroic mirror from the first surface to the second surface was designed to take place in this wavelength range to have minimum interference from the likely Na emission.

In theory, the use of wide measurement bands, a practical necessity due to the limited CCD sensitivity, decreases the accuracy of the two-color pyrometric temperature measurement, but on the other hand, it makes the measurement less sensitive to interference from individual spectral lines.

Figure 12 shows an example of particle temperature and velocity measurements from plasma spraying experiments using Al_2O_3 and NiCrAlY powders. The spray parameters were given in Table 4. The camera exposure time for faster Al_2O_3 particles was $5 \mu\text{s}$ and for NiCrAlY, it was $7 \mu\text{s}$. The imaged region in the plasma plume was in both cases $28.0 \times 22.4 \text{ mm}$. The center of the imaged region was located at the spray distance (Table 4).

In Fig. 12, the distributions are calculated from 200 frames for Al_2O_3 , the corresponding total number of accepted particles being 4854. For NiCrAlY, the data are calculated from 100 frames and 341 particles.

Figure 13 shows schematically the determination of lateral particle parameter distributions by dividing the recorded image vertically into smaller sections.

Figure 14 shows an example of lateral temperature, velocity, and particle count distributions for Al_2O_3 . In this figure, the center column shows results recorded with standard spray parameters (Table 4), and the left and right columns show results obtained when the carrier gas flow rate was changed $\pm 20\%$ from the standard setting. From Fig. 14, it can be seen that the carrier gas flow rate clearly affects the total number of detected particles^[6-8] and also the corresponding lateral particle distribution. In this case, the particle feed was from the direction corresponding to the highest pixel values in the x -axis of the graphs. It should be noted that the lateral particle distribution is based purely on the number of the detected particles and is thus more informative than a simple brightness distribution of the plume. A clear effect of carrier gas flow rate adjustments can be seen, too, in the particle velocity distributions, the corresponding change in the temperature values being not so distinct.

The black dots marked in the temperature and velocity distributions in Fig. 14 show corresponding point measured average values recorded during the same test runs using a

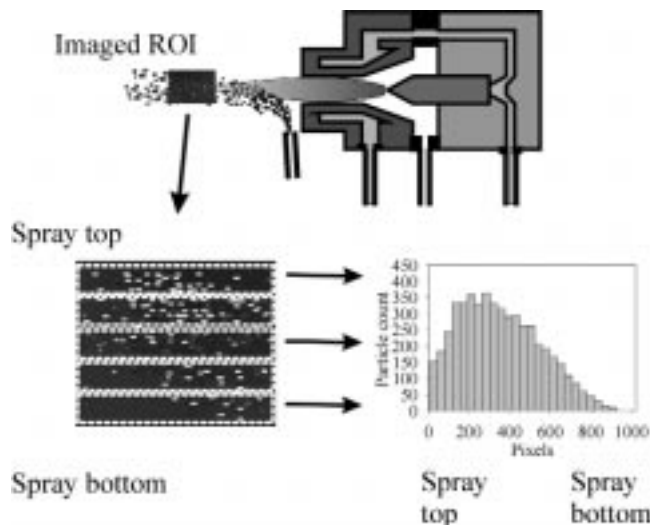


Fig. 13 Division of imaged region of interest (ROI) into smaller sections for determination of lateral particle parameter distributions. X-axis values of the lateral distribution are given in detector pixel values

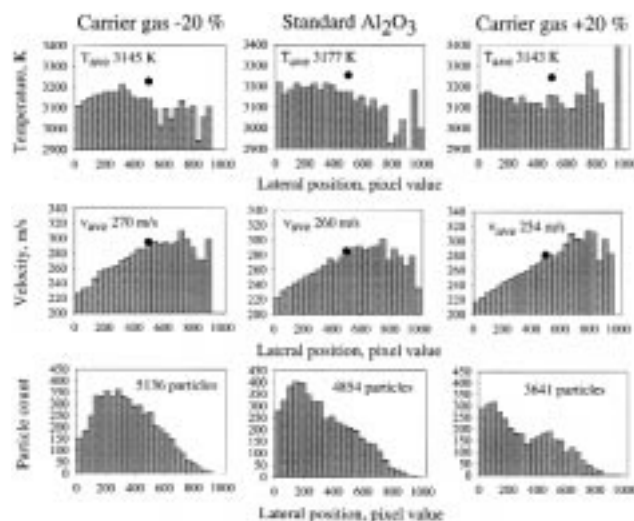


Fig. 14 Lateral temperature, velocity and particle count distributions of plasma sprayed Al_2O_3 powder. The centre column shows results for standard spray parameters given in Table 4. Left column recorded with carrier gas flow reduced 20%, and right column with carrier gas flow rate increased 20%. Average values of temperature and velocity are marked in the graphs together with the total number of the detected particles per measurement including 200 frames. The meaning of the black dots in the velocity and temperature distributions is explained in the text. On x -axis scale 1024 pixels correspond to 22.4 mm in real physical dimensions.

commercial optical in-flight particle sensor (DPV-2000, Tecnar Automation, Québec, Canada). The measurement volume ($<1 \text{ mm}^3$) of this sensor was located in the center of the imaged area and on the centerline of the plasma plume. The velocities measured by both methods show good correlation. The correlation in the particle temperatures is not equally good, but it should be kept in mind that these instruments measure a different group of

particles due to the differences in the validation of the detected particles. The slightly lower detection sensitivity of the prototype imaging system presumably excludes the smallest and hottest particles, thus lowering the measured average temperatures. Measurement systems use different measurement wavelengths and systems were also calibrated independently using different calibration sources. The prototype was calibrated against a tungsten ribbon lamp (Osram W17G, München, Germany), and no additional correction for emissivity as a function of wavelength or temperature was applied in these preliminary tests.

5. Discussion and Conclusions

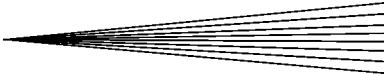
The aim of this work has been to investigate the possibilities of developing a rugged, simple passive imaging instrument, which can provide visual information of the spray plume in combination with quantitative evaluation of the most important spray particle parameters. Thus, the aims of the design have been to achieve system simplicity and low cost rather than to achieve maximum scientific accuracy in the particle parameter determination. Large measurement area compared to point measurements provides an overview of the state of the process, and information from a representative group of particles, and thus has potential for better sensitivity in detecting significant deviations in the spray process.

The instrument presented here can be readily used to determine velocity and temperature distributions from individual in-flight particles. Spatial distributions of these particle parameters can be presented by dividing the imaged area into smaller sections. Particle velocity and temperature information is comparable between different spray processes and spray materials. However, it should be kept in mind that changes in the particle detection criteria also have an effect on the detection limits, and this can further affect the recorded parameter distributions.

Keeping the optical settings and particle detection criteria unchanged, the number of detected particles per frame, relative brightness of the particles, and direction of the particle movement (angle respect to the detection system) can be used to monitor the state of a given spray process together with the particle velocity and temperature information. Empirical knowledge of these parameters can be utilized to optimize the process, or their temporal behavior can be used to ensure continuous coating quality.^[6] Due to the imaging principle, it is also possible to obtain information from collisions between the in-flight particles and from the appearance of possible vaporized particle material.

In the line-of-sight direction, the effective measurement volume is defined by discriminating out-of-focus particles based on their signal traces, as described in Section 3.2. Thus, the measurement volume has a typical depth of plus or minus a few millimeters in respect to the focus plane depending on the aperture settings of the optics. This provides measurement information from a limited three-dimensional volume, but in practice also the detection limit and accuracy change slightly as a function of the amount of deviation from the focus.

The accuracy of the temperature measurements using the very first prototype system was discussed in Section 4. Considering the measurement apparatus itself, the ultimate temperature measurement accuracy is mostly limited due to the nonideal



CCD detector characteristics described in Section 2.3. The fast development of the detector technologies is prone to give new possibilities to realize some improvements in this respect in the future. Use of more sophisticated calculation algorithms could also be used to further compensate for those uncertainties in the determined signals, which are caused by the distribution of the single particle images onto varying amount of pixels. The future progress in the power of personal computers can be used to increase significantly the frame processing rate even if more complicated calculation algorithms are adopted. The performance of the optics of the prototype can also be significantly improved by the use of a higher quality lens system, which is better optimized to work together with the dichroic double mirror.

The approach to combine measurement of multiple in-flight particle parameters in a single passive instrument is advantageous considering industrial on-line process monitoring applications. The physical size of the equipment should be made compact, which is important in applications where the optical head should be attached directly to the torch manipulated by a robotic system. The size of this type of an imaging system can be made reasonably compact, the limiting factor being the size of the optical parts rather than the size of the camera and electronics.

The ultimate accuracy of the single, passive imaging instrument in determining the various single particle parameters will fundamentally be more limited than the accuracy of methods specialized for a certain particle parameter or of methods using external illumination. Nevertheless, the method developed in this work seems to offer some interesting and promising possibilities for future on-line process optimization and monitoring purposes.

Acknowledgments

The contribution of technician Antti Lepistö in constructing the hardware of the prototype system is gratefully acknowledged. The authors thank Mr Gérard Barbezat, Sulzer Metco AG, for kindly providing the possibility of testing the prototype system at Sulzer Metco (Wohlen, Switzerland). Tekes, the National Technology Agency of Finland, is acknowledged for financial support of this work.

References

1. C. Moreau: in *Thermal Spray: Meeting the Challenges of the 21st Century*, C. Coddet, ed., ASM International, Materials Park, OH, 1998, pp. 1681-93.
2. P. Fauchais, J.F. Coudert, and M. Vardelle: *Plasma Diagnostics*, Academic Press, New York, NY, 1989, pp. 349-445.
3. J.R. Fincke, W.D. Swank, and C.L. Jeffrey: *IEEE Trans. Plasma Sci.*, 1990, vol. PS-18, pp. 948-57.
4. T.T. Hoffman and J. Agapakis: *J. Thermal Spray Technol.*, 1992, vol. 1 (1), pp. 19-25.
5. T. Sakuta and M. Boulos: *Rev. Scientific Instruments*, 1988, vol. 59 (2), pp. 285-91.
6. J. Vattulainen, J. Knuutila, T. Lehtinen, T. Mäntylä, and R. Hernberg: in *Thermal Spray: Meeting the Challenges of the 21st Century*, C. Coddet, ed., ASM International, Materials Park, OH, 1998, pp. 767-72.
7. J. Knuutila, P. Saarenrinne, R. Hernberg, T. Lehtinen, and T. Mäntylä: in *Thermal Spray: United Conf. Proc.*, C.C. Berndt, ed., ASM International, Materials Park, OH, 1997, pp. 577-82.

8. T. Lehtinen, J. Knuuttila, J. Vattulainen, T. Mäntylä, and R. Hernberg: in *Thermal Spray: Practical Solutions for Engineering Problems*, C.C. Berndt, ed., ASM International, Materials Park, OH, 1996, pp. 525-30.
9. W.D. Swank, J.R. Fincke, and D.C. Haggard: in *Thermal Spray Science & Technology*, C.C. Berndt and S. Sampath, eds., ASM International, Materials Park, OH, 1995, pp. 111-16.
10. T.J. Quinn: *Temperature*, Academic Press, London, 1983.
11. S. Coulombe, M.I. Boulos, and T. Sakuta: *Measurement Sci. and Technol.*, 1995, vol. 6, pp. 383-90.
12. C. Moreau, M. Lamontagne, and P. Cielo: "Method and Apparatus for Monitoring the Temperature and Velocity of Plasma Sprayed Particles," U.S. Patent 5,180,921, 1993.
13. <http://www.pco.de/>, Sencicam SVGA Digital Camera Datasheets, PCO Computer Optics GmbH, 93309 Kelheim, Germany, 1999.
14. G.E. Healey and R. Kondepudy: *IEEE Trans. Pattern Analysis Machine Intelligence*, 1994, vol. 16 (3), pp. 267-76.
15. R.A. Boie and I.J. Cox: *IEEE Trans. Pattern Analysis Machine Intelligence*, 1992, vol. 14 (6), pp. 671-78.
16. P. Gougeon and C. Moreau: *J. Thermal Spray Technol.*, 1993, vol. 2, pp. 229-34.
17. J. Mishin, M. Vardelle, J. Lesinski, and P. Fauchais: *J. Phys. E: Scientific Instruments*, 1987, vol. 20, pp. 620-25.
18. <http://www.specim.fi/>, ImSpector Spectrograph Datasheets, Spectral Imaging Ltd., FIN-90571 Oulu, Finland, 1999.
19. T. Joutsenoja, J. Stenberg, R. Hernberg, and M. Aho: *Appl. Optics*, 1997, vol. 30, pp. 1525-35.